Simulation and Characterization of Interfacial Wave Breakup in Airblast Atomization

Delin Jiang[1], Yue Ling[*1]

[1]Department of Mechanical Engineering, Baylor University, Waco, TX, USA
*Corresponding author email: Stanley_Ling@baylor.edu

Abstract
In airblast atomization, the shear between the fast gas and slow liquid streams triggers an interfacial instability. The instability develops into interfacial waves that grow and propagate downstream. The longitudinal and transverse instabilities have a strong influence on the development and breakup of the interfacial waves and also the resulting spray characteristics. While extensive previous studies have been dedicated to the longitudinal instability, less attention has been paid on the traverse development of the interfacial waves. This paper aims at investigating the development of the interfacial waves when turbulent fluctuations are present in the gas inlet, through direct numerical simulation. The mass-momentum consistent volume-of-fluid method has been be used to capture the sharp interface. Turbulent velocity fluctuations are introduced at the gas inlet through a digital filter method. The effect of the inlet gas turbulence intensity on the dominant longitudinal wave frequency and the transverse wave number is characterized by a parametric study.

Keywords
Airblast atomization, direct numerical simulation, interfacial instability

Introduction

Atomization is the process of breaking bulk liquid into small droplets and is important to various industry applications, e.g. aerospace, automobile and painting. A comprehensive understanding of atomization process and a capability to accurately predict the spray characteristics are essential to many spray applications. Among different atomization approaches, airblast atomization [1] is an effective method to produce fine sprays and is widely used in fuel injection systems. In airblast atomization, the fast gas stream interacts with the parallel co-flowing liquid stream of lower velocity, the gas-liquid interface is unstable and interfacial waves will form.

The formation and early development of the interfacial waves are mainly controlled by the longitudinal shear-induced Kelvin-Helmholtz like instability. The most unstable mode in the longitudinal instability dictates the frequency and the wavelengths of the interfacial waves. Linear stability analysis has been carried out to predict the most-unstable longitudinal wave frequency and the growth rate. While inviscid analysis [2, 3] yielded reasonable predictions for the frequency but under-predicted the spatial growth rate, viscous temporal analysis [4] well predicted the growth rate but overestimated frequency. It was later shown that viscous spatial-temporal stability analysis is required to well predict both the frequency and the growth rate [5, 6].

Conventionally, stability analysis and numerical studies of the longitudinal instability assume that, both the gas and liquid streams are laminar when they meet [5, 6, 7, 8]. Nevertheless, turbulent fluctuations may exist in the gas stream in experiment due to the high Reynolds number. The gas inlet turbulence has been shown to have a strong impact on the longitudinal instability [9, 10]. Both the frequency and the spatial growth rate were observed to increase approximately linearly with the inlet gas turbulence intensity I, when I is over a threshold [10]. Attempts have been made to incorporate the effect of inlet gas turbulence in the linear viscous spatial-temporal stability analysis using turbulent viscosity models. The modified stability analysis reasonably capture the trend that the frequency and the growth rate increase with I but underestimates the

values [10]. An accurate linear stability theory that can capture the most unstable modes for a turbulent gas stream remain to be developed.

Transverse modulations of the longitudinal waves develop when the waves grow and propagate downstream, turning the interfacial waves to completely 3D. Compared to the longitudinal waves, the formation mechanisms for the transverse waves are less understood. The Rayleigh-Taylor (RT) instability has been suggested to be the primary driving mechanism for the transverse instability in a cylindrical coaxial configuration [2]. When the interface accelerates from the gas toward the liquid due to the longitudinal instability, the transverse instability is triggered and the most-unstable wavelength is estimated through RT theory. Since the transverse instability is closely tied to the longitudinal counterpart and the latter is influenced by the inlet gas turbulence, it is expected that the inlet gas turbulence will also play a significant role in the transverse instability and the resulting modulations of the interfacial waves. A detailed analysis on the effect of inlet gas turbulence on transverse instability remains absent.

There exist multiple pathways by which subsequent breakup of the 3D interfacial waves to filaments and droplets: the fingering and the hole-in-sheet modes [7]. The fingering modes typically occur when the disintegration of the 3D interfacial wave is relatively mild. In such a case, the Rayleigh-Plateau (RP) instability gets a chance to develop at the Taylor-Culick rim formed at the edge of the liquid sheet [11]. The RP instability results in liquid fingers extended from the rim along the streamwise direction. The number of fingers formed is similar to the transverse wavenumber [2]. The liquid fingers or filaments will continue to break into droplets. The size distribution of droplets formed is essential to spray applications and different distribution models, including the most popular log-normal and Gamma distribution models, have been proposed [12, 13].

When long liquid sheets extend from the interfacial wave crest and has a strong interaction with the gas stream, the disintegration of the interfacial wave is generally more violent and will then follow the hole-in-sheet mode [7]. The hole expansion speed follows the Taylor-Culick velocity [14, 7]. The holes grow and eventually lead to a violent rupture of the sheet, producing separate ligament, droplets of different sizes and orientations and fingers that remain attached to the liquid sheet. The formation of a hole in the liquid sheet is due to the pinching of the two surfaces of the liquid sheet. In numerical simulations, the cell size serves as the numerical cut-off length scale to pinch a liquid sheet and to change the topology. Former studies on the interfacial waves breakup assumes the co-flowing gas stream is laminar. The effect of the inlet gas turbulence on the breakup mode of the interfacial waves and the droplets statistics remains unclear.

The goal of the present study is to simulate and to characterize the development and breakup of the interfacial waves in airblast atomization through direct numerical simulations. The focus is on the interfacial instability and the effect of inlet gas turbulence. To allow a detailed investigation of the transverse features of interfacial waves, we have used a computational domain that is three times as wide (in transverse direction) as that in former studies [8, 10].

Simulation Methods

Governing equations

The two-phase interfacial flows are governed by the incompressible Naviers-Stokes equations with surface tension,

$$\rho\left(\frac{\partial u_i}{\partial t}+u_i\frac{\partial u_j}{\partial x_j}\right)=-\frac{\partial p}{\partial x_i}+\frac{\partial}{\partial x_j}\left[\mu\left(\frac{\partial u_i}{\partial x_j}+\frac{\partial u_j}{\partial x_i}\right)\right]+\sigma\kappa\delta_s n_i\,, \tag{1}$$

$$\frac{\partial u_i}{\partial x_i}=0\,. \tag{2}$$

where ρ, u_i, p, μ represent density, velocity, pressure and viscosity, respectively. The Dirac distribution function δ_s is localized on the interface. The surface tension is denoted by σ, while κ and n_i represent the curvature and normal vector of the interface.

The gas and liquid phases are distinguished by the liquid volume fraction c, the evolution of which follows the advection equation:

$$\frac{\partial c}{\partial t} + u_i \frac{\partial c}{\partial x_i} = 0\,. \tag{3}$$

Numerical solver

The governing equations above are solved using the finite volume method on a staggered grid. The advection equation Eq. (3) is solved using a geometric volume-of-fluid (VOF) method. The interface normal is computed by following the mixed Young's-centred method and the Lagrangian-explicit scheme is used for the VOF advection [15]. The convection term in the momentum equation, Eq.(1), is discretized consistently with the VOF method [16]. The incompressibility condition is incorporated using the projection method. The pressure Poisson equation is solved using PFMG multigrid solver in the HYPRE library. The balanced-force continuous-surface-force formulation is used to calculate the surface tension and the interface curvature is evaluated using the height-function method [17]. The time integration is done by a second-order predictor-corrector method. The aforementioned numerical methods have been implemented in the open-source solver, *PARIS-Simulator* [18], which is used for the present simulations.

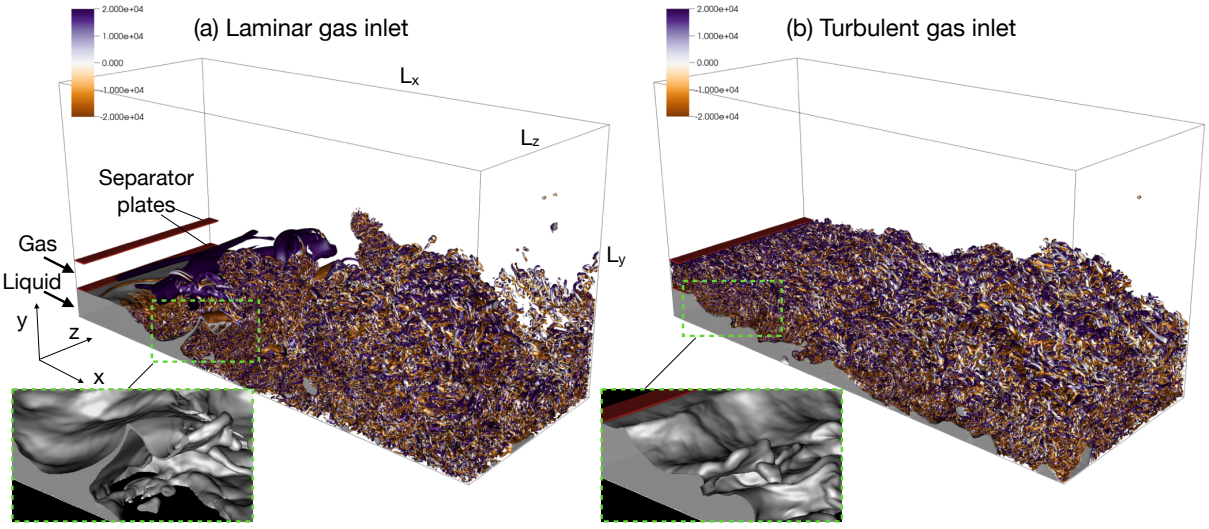

Figure 1. Airblast atomization of a planar liquid jet with (a) laminar and (b) turbulent co-flowing gas streams. The turbulent vortical structures are visualized by the iso-surface of $\lambda_2 = -10^{-8}$ colored by $z-$vorticity.

Simulation setup

The simulation domain is a rectangular box as shown in figure 1. The liquid and gas streams gradually enter the domain from the left. Two plates are introduced to separate the gas and liquid streams near the inlet. The bottom surface is a slip wall. Periodic boundary conditions are applied to the front and back surfaces. The free boundary condition is invoked at the top to allow the gas to freely flow through the boundary. The velocity outflow boundary condition is imposed at the right surface. The mean flow at the inlet is horizontal, and the x-component is specified as

$$\overline{u}_0(y) = \begin{cases} U_l \,\mathrm{erf}\left[\frac{H-y}{\delta}\right], & 0 \le y < H \text{ (liquid stream)}, \\ 0, & H \le y < H+\eta_y \text{ (separator plate)}, \\ U_g \,\mathrm{erf}\left[\frac{y-(H+\eta_y)}{\delta}\right] \mathrm{erf}\left[\frac{2H-y}{\delta}\right], & H+\eta_y \le y < 2H \text{ (gas stream)}, \\ 0, & \mathrm{else} \text{ (separator plate \& no-slip wall)}, \end{cases} \tag{4}$$

Table 1. Physical parameters.

ρ_l	ρ_g	μ_l	μ_g	σ	U_l	U_g	H	δ
(kg/m^3)	(kg/m^3)	(Pa s)	(Pa s)	(N/m)	(m/s)	(m/s)	(mm)	(mm)
1000	50	10^{-3}	5×10^{-5}	0.05	0.5	10	0.8	0.1

Table 2. Key dimensionless parameters.

M	r	m	$\mathrm{Re}_{g,\delta}$	$\mathrm{We}_{g,\delta}$	$\mathrm{Re}_{g,H}$	I
$\rho_g U_g^2/(\rho_l U_l^2)$	ρ_l/ρ_g	μ_l/μ_g	$\rho_g U_g \delta/\mu_g$	$\rho_g U_g^2 \delta/\sigma$	$\rho_g U_g H_g/\mu_g$	$(\sqrt{\overline{u'u'}})_e/U_g$
20	20	20	1000	10	7750	$0, 0.06, 0.13$

where U_l and U_g are the liquid and gas velocities away from the separator plates, respectively. The error functions erf are used to model the boundary layers and the parameter δ characterizes the boundary layer thickness. Pseudo turbulent velocity fluctuations u', v', w' are computed using the digital filter approach [19] at the gas inlet (*i.e.*, $H + \eta_y \leq y < 2H$), so the total velocity will be the sum of the mean and the fluctuations. The root mean square of u' at the center of the gas stream ($y = 1.5H$) and the exit of the separator plate ($x = \eta_x$), normalized by U_g, is defined as the intensity of the inlet gas turbulence, *i.e.*, $I = (\sqrt{\overline{u'u'}})_e/U_g$.
Important physical parameters for simulation setup are summarized in Table 1. The height of the liquid stream H is taken as the characteristic length scale. The dimensions of the two thin plates are the same and have the thickness of $\eta_y = H/32$ and the length of $\eta_x = H/2$. The length (L_x), height (L_y), and width (L_z) of the domain are $16H$, $8H$ and $6H$, respectively. Key dimensionless parameters are listed in Table 2. Applying H and U_g as the scaling variables, the dimensionless time, velocity, and length are defined as $t^* = tU_g/H$, $u^* = u/U_g$, $x^* = x/H$. The domain is discretized using a fixed regular cubic grid. The cell size is $\Delta = H/128 = 6.25$ µm and the total number of cells are about 1.6 billion. Three different values of I are considered, see table 3. The simulations are performed using 64 Intel Xeon Platinum 8160 nodes (equivalent to 3072 cores) on the TACC Stampede2. The total computational cost for the present simulations is about 200,000 node-hours.

Table 3. Summary of simulation cases.

Case	W1	W2	W3
I	0	0.06	0.13

Results and discussion

General behavior

Figures 1(a) and (b) represent snapshots of the liquid and turbulent gas flows for case W0 and W2. The λ_2 criterion has been used to visualize the turbulent vortical structures. The iso-surfaces of $\lambda_2 = -10^{-8}$ are colored by $z-$vorticity. The positive (purple) and negative (orange) values indicate that the vortices of different rotational directions. Due to the higher velocity of the gas stream, the top and bottom boundaries of the gas stream are unstable, which develop into gas-gas and gas-liquid mixing layers. For the case W0, vortex tubes can be recognized in the gas-gas mixing layer near the inlet, though the whole gas stream transits to fully turbulent further downstream. For the case W2, the turbulence introduced in the inlet is observed to continue to develop along the stream. This indicates the approach to introduce turbulent fluctuations at the inlet is effective. For both cases, The shear between the gas and liquid streams triggers a Kelvin-Helmholtz longitudinal instability, which is the onset of the

formation of interfacial waves.

Longitudinal instability and wave formation

To characterize the longitudinal instability, the interfacial height is measured at $x^* = 0.625$ and the temporal evolution of the interfacial height is shown in figure 2(a) for all three cases. As I increases, the wave amplitude increases. A dominant mode can be recognized. Fourier transforms are then performed to generate the frequency spectra and to identify the frequency of the dominant mode, see Fig. 2(b). It is observed that the dominant frequency ω increases with I. The variation of the frequency over I are shown in Fig. 2(c), compared to the experimental data of Matas *et al.* [9]. Here the frequency is normalized by the value at $I = 0$. It is seen that increase of ω over I agree reasonably well with than the experimental results. The density and viscosity ratios, r and n in the experiment are higher than those used in the simulation, which may have contributed to the discrepancy.

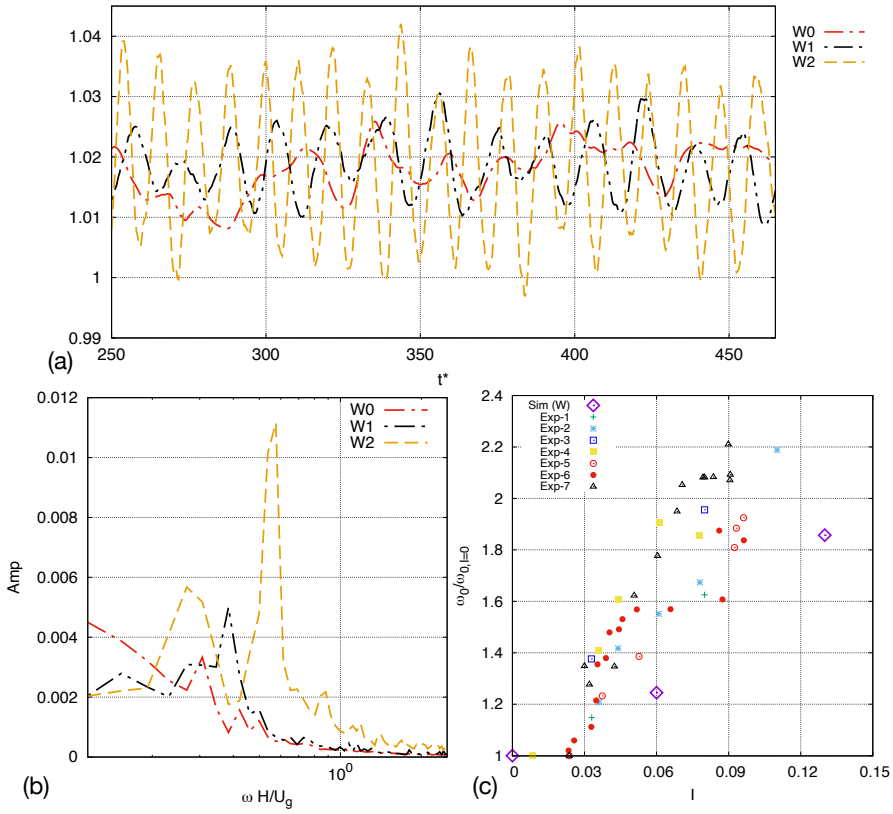

Figure 2. a): temporal evolution of interfacial variation at $x^* = 0.625H$. (b): frequency spectrum that corresponds to data in (a). (c): Comparison of normalized dominant frequency, conducted simulation and experimental data ([9]).

Transverse instability and wave development

To investigate the transverse instability and interfacial modulations, the dominant transverse wavenumber for the interfacial height, $k_{\max}$, is plotted as function of t^* and x^* in Fig. 3. For a given t^* and x^*, Fourier transform is performed for the interface height over the transverse coordinate, *i.e.*, $h(z^*)$. Then the wavenumber corresponding to the maximum amplitude, $k_{\max}$, is measured. It is observed that $k_{\max}$ rises to much larger values when a longitudinal wave passes by. The trajectories of the longitudinal waves appear as inclined lines of high $k_{\max}$, the slopes of which represent the interfacial wave propagation speed, which is found to agree well with the Dimotakis speed U_D. This suggests that the formation of transverse modulations on the interface is associated with development of the longitudinal waves. The reason is that the transverse interfacial modulation is due to the RT instability, which is in turn induced by

the longitudinal instability. Therefore, only $k_{\max}$ at the longitudinal wave location in the map corresponds to the transverse wavenumber of the interfacial wave, denoted by k_T.

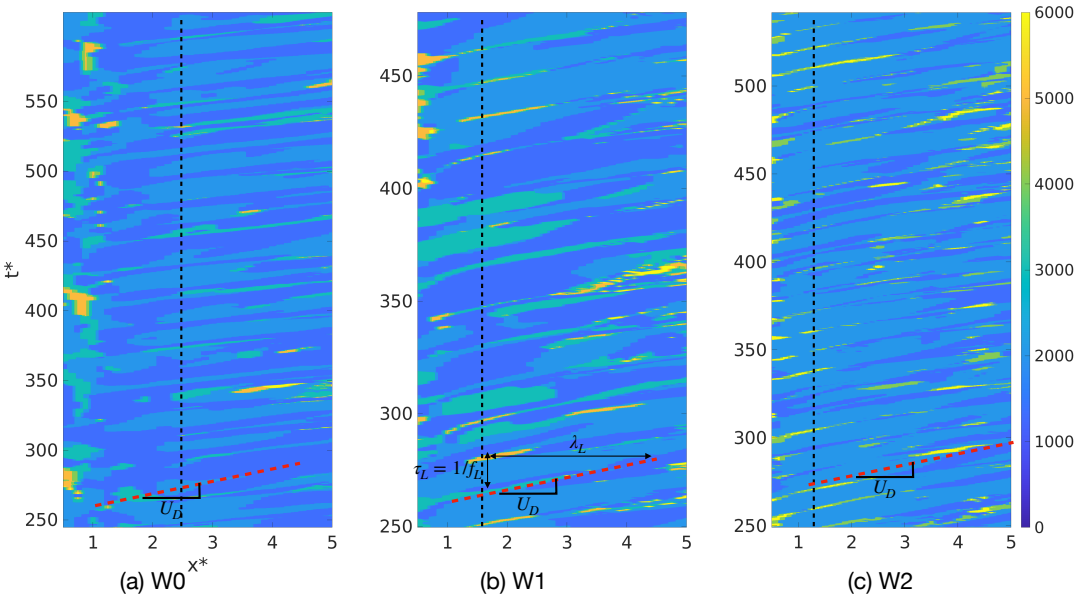

Figure 3. The x^*-t^* map for the dominant transverse wavenumber $k_{\max}$ for cases (a) W0, (b) W1, and (c) W2.

The temporal evolutions of $k_{\max}$ for different I are shown in Figs. 4(a-c). The data is collected at the streamwise location $x^* = 2.375$, 1.625, 1.25, for $I = 0$, 0.07, 0.13, respectively, see the dashed lines in Fig. 3, where the longitudinal wave amplitudes are similar. The RT theoretical predictions are also shown for comparison. The location of the longitudinal waves are indicated by the vertical lines according to the dominant longitudinal frequency ω_L^*. The time-average $\overline{k}_T$ is shown in Fig. 4(d) and is observed to increase from about 3300 to about 5100 when I increases from 0 to 0.13. The RT model predictions generally agree well with the simulation results.

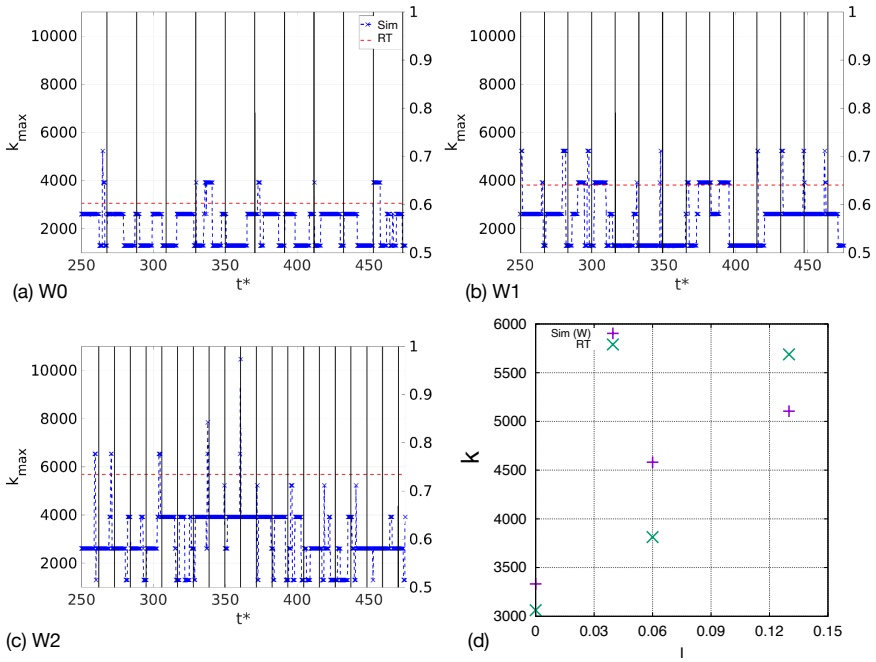

Figure 4. (a): Temporal evolution of dominant wave number $k_{\max}$ for cases (a) W0, (b) W1, and (c) W2. (d) The time-average $\overline{k}_T$ as a function of I, compared with the RT theory.

Breakup of interfacial waves

Furthermore, the inlet gas turbulence also has a strong impact on breakup dynamics of the interfacial waves. The number of holes formed on the sheet, and when and where the holes are formed for the cases W0 and W2 are different. The sequential snapshots for the interface colored by the x-velocity are shown in Fig. 5 to demonstrate the typical breakup of the liquid waves for the two cases with different I. The holes arise further downstream for the case W0, and multiple holes form simultaneously behind the rim of the liquid sheet. The holes expand and merge, and eventually the rim is detached from the liquid sheet, forming a filament aligned with the transverse direction. For the case W2, the rims on the edge of the waves are more irregular. The number of holes is significantly lower than that for the case W0. The expansion of the holes leads to fingers align with the longitudinal direction. The finger diameter is significantly larger than that for the filament formed for case W0. The different breakup dynamics significantly influences the statistics of the droplets formed. The number of droplets formed for the case W2 is significantly lower and the mean droplet size is larger, compared to the case W0.

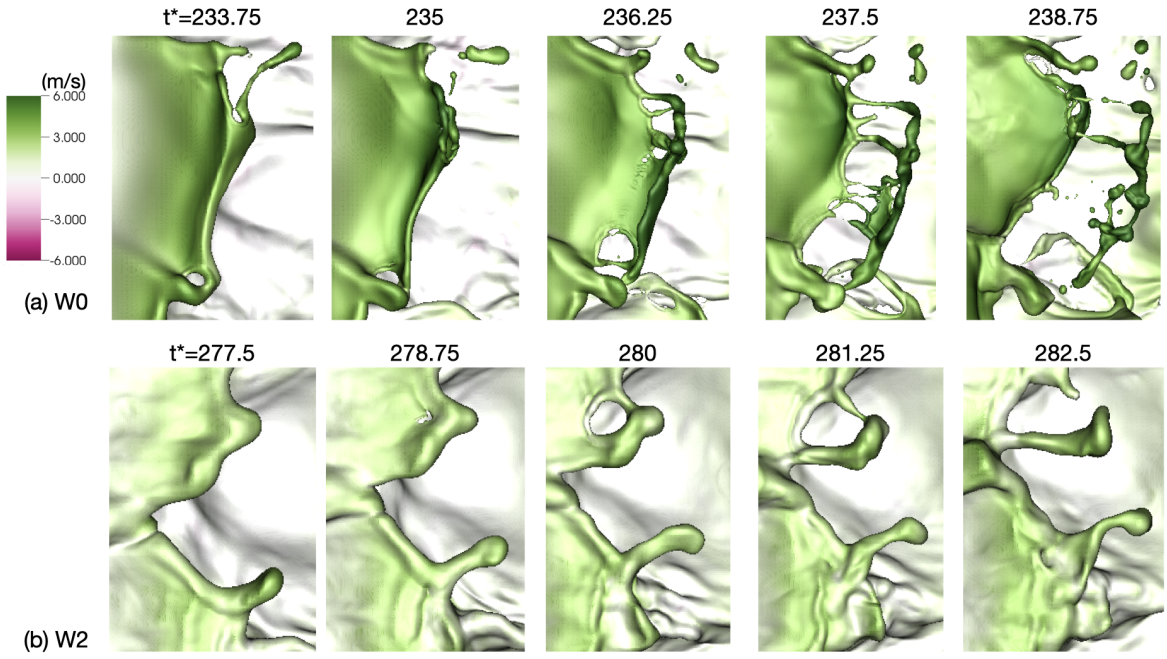

Figure 5. Disintegration of the liquid waves for the cases (a) W0 and (b) W2. The interfaces colored with x-velocity

Conclusions

The development and breakup of interfacial waves in airblast atomization are investigated through direct numerical simulation. The effect of the inlet gas turbulence on the longitudinal and transverse interfacial instability is characterized through a parametric study. Both the longitudinal frequency and the transverse wavenumber increase with the turbulence intensity I at gas inlet. The turbulence modulation of interfacial waves formation and development also impact the eventual breakup of the interfacial waves and the statistics of the droplets formed.

Acknowledgements

This research is supported by the National Science Foundation (#1942324). The authors also acknowledge the Extreme Science and Engineering Discovery Environment (XSEDE) for providing the computational resources that have contributed to the research results reported in this paper. The Baylor High Performance and Research Computing Services (HPRCS) have been used to process the simulation results.

References

[1] Lefebvre, A. H. "Airblast atomization." *Prog. Energ. Combust. Sci.* Vol. 6 (1980): pp. 233–261.

[2] Marmottant, P. and Villermaux, E. "On spray formation." *J. Fluid Mech.* Vol. 498 (2004): pp. 73–111.

[3] Matas, J.-P., Marty, S. and Cartellier, A. "Experimental and analytical study of the shear instability of a gas-liquid mixing layer." *Phys. Fluids* Vol. 23 (2011): p. 094112.

[4] Boeck, T. and Zaleski, S. "Viscous versus inviscid instability of two-phase mixing layers with continuous velocity profile." *Phys. Fluids* Vol. 17 (2005): p. 032106.

[5] Otto, T., Rossi, M. and Boeck, T. "Viscous instability of a sheared liquid-gas interface: Dependence on fluid properties and basic velocity profile." *Phys. Fluids* Vol. 25 (2013): p. 032103.

[6] Fuster, D., Matas, J. P., Marty, S., Popinet, S., J., Hoepffner, Cartellier, A. and Zaleski, S. "Instability regimes in the primary breakup region of planar coflowing sheets." *J. Fluid Mech* Vol. 736 (2013): pp. 150–176.

[7] Ling, Y., Fuster, D., Zaleski, S. and Tryggvason, G. "Spray formation in a quasiplanar gas-liquid mixing layer at moderate density ratios: A numerical closeup." *Phys. Rev. Fluids* Vol. 2 (2017): p. 014005.

[8] Ling, Y., Fuster, D., Tryggvasson, G. and Zaleski, S. "A two-phase mixing layer between parallel gas and liquid streams: multiphase turbulence statistics and influence of interfacial instability." *J. Fluid Mech.* Vol. 859 (2019): pp. 268–307.

[9] Matas, J.-P., Marty, S., Dem, M. S. and Cartellier, A. "Influence of Gas Turbulence on the Instability of an Air-Water Mixing Layer." *Phys. Rev. Lett.* Vol. 115 (2015): p. 074501.

[10] Jiang, D. and Ling, Y. "Destabilization of a planar liquid stream by a co-flowing turbulent gas stream." *Int. J. Multiphase Flow* Vol. 122 (2020): p. 103121.

[11] Agbaglah, G., Josserand, C. and Zaleski, S. "Longitudinal instability of a liquid rim." *Phys. Fluids* Vol. 25 (2013): p. 022103.

[12] Sotolongo-Costa, O., Moreno-Vega, Y., Lloveras-González, J. J. and Antoranz, J. C. "Criticality in Droplet Fragmentation." *Phys. Rev. Lett.* (1996): pp. 42–45.

[13] Villermaux, E., Marmottant, Ph. and Duplat, J. "Ligament-mediated spray formation." *Phys. Rev. Lett.* Vol. 92 (2004): p. 074501.

[14] Opfer, L., Roisman, I. V., Venzmer, J., Klostermann, M. and Tropea, C. "Droplet-air collision dynamics: Evolution of the film thickness." *Phys. Rev. E* Vol. 89 (2014): p. 013023.

[15] Scardovelli, R. and Zaleski, S. "Interface reconstruction with least-square fit and split Eulerian–Lagrangian advection." *Int. J. Numer. Meth. Fluids* Vol. 41 No. 3 (2003): pp. 251–274.

[16] Arrufat, T., Crialesi-Esposito, M., Fuster, D., Ling, Y., Malan, L., Pal, S., Scardovelli, R., Tryggvason, G. and Zaleski, S. "A momentum-conserving, consistent, Volume-of-Fluid method for incompressible flow on staggered grids." *Comput. Fluids* Vol. 215 (2020): p. 104785.

[17] Popinet, S. "An accurate adaptive solver for surface-tension-driven interfacial flows." *J. Comput. Phys.* Vol. 228 No. 16 (2009): pp. 5838–5866.

[18] Aniszewski, W., Arrufat, T., Crialesi-Esposito, M., Dabiri, S., Fuster, D., Ling, Y., Lu, J., Malan, L., Pal, S., Scardovelli, R., Tryggvason, G., Yecko, P. and Zaleski, S. "PArallel, Robust, Interface Simulator (PARIS)." *Comput. Phys. Comm.* Vol. 10.1016/j.cpc.2021.107849.

[19] Klein, M., Sadiki, A. and Janicka, J. "A digital filter based generation of inflow data for spatially developing direct numerical or large eddy simulations." *J. Comput. Phys.* Vol. 186 (2003): pp. 652–665.